Growth rates of dry thermal oxidation of 4H-silicon carbide

V. Šimonka, A. Hössinger, J. Weinbub, and S. Selberherr

Citation: Journal of Applied Physics **120**, 135705 (2016);
View online: https://doi.org/10.1063/1.4964688
View Table of Contents: http://aip.scitation.org/toc/jap/120/13
Published by the American Institute of Physics

Growth rates of dry thermal oxidation of 4H-silicon carbide

V. Šimonka,[1,a)] A. Hössinger,[2] J. Weinbub,[1] and S. Selberherr[3]
[1]*Christian Doppler Laboratory for High Performance TCAD, Institute for Microelectronics, TU Wien, Gußhausstraße 27-29/E360, 1040 Wien, Austria*
[2]*Silvaco Europe Ltd., Compass Point, St Ives, Cambridge PE27 5JL, United Kingdom*
[3]*Institute for Microelectronics, TU Wien, Gußhausstraße 27-29/E360, 1040 Wien, Austria*

(Received 13 July 2016; accepted 28 September 2016; published online 7 October 2016)

We provide a full set of growth rate coefficients to enable high-accuracy two- and three-dimensional simulations of dry thermal oxidation of 4H-silicon carbide. The available models are insufficient for the simulation of complex multi-dimensional structures, as they are unable to predict oxidation for arbitrary crystal directions because of the insufficient growth rate coefficients. By investigating time-dependent dry thermal oxidation kinetics, we obtain temperature-dependent growth rate coefficients for surfaces with different crystal orientations. We fit experimental data using an empirical relation to obtain the oxidation growth rate parameters. Time-dependent oxide thicknesses at various temperatures are taken from published experimental findings. We discuss the oxidation rate parameters in terms of surface orientation and oxidation temperature. Additionally, we fit the obtained temperature-dependent growth rate coefficients using the Arrhenius equation to obtain activation energies and pre-exponential factors for the four crystal orientations. The thereby obtained parameters are essential for enabling high-accuracy simulations of dry thermal oxidation and can be directly used to augment multi-dimensional process simulations. *Published by AIP Publishing.*
[http://dx.doi.org/10.1063/1.4964688]

I. INTRODUCTION

Thermally grown silicon dioxide (SiO_2) plays a unique role in the device fabrication technology as an insulating layer. Among the wide band gap semiconductors, silicon carbide (SiC) is the only compound semiconductor that can be thermally oxidized in the form of SiO_2, similar to silicon (Si). Although Si has been used as a power device semiconductor, significant performance improvements of Si devices can no longer be expected because the devices have reached their performance limit introduced by the physical properties of Si. The devices that can be fabricated on Si substrates (e.g., power metal-oxide-semiconductor field-effect transistors, insulated-gate bipolar transistors) can also be fabricated on the SiC substrates. Therefore, SiC is considered to be a post Si power device material, as SiC offers superior physical properties over Si, such as wide band gap, high electrical breakdown voltage, and high thermal conductivity.[1]

The most promising polytypes for SiC are 3C-, 4H-, 6H-, and 15R-SiC.[1] These polytypes are characterized by the stacking sequence of the bi-atom layers of the SiC structure. Changing the sequence has a profound effect on the electrical properties.[2] The 4-bilayer 4H-SiC recently received most attention regarding its oxidation mechanisms;[3–7] therefore, we explicitly focus on the 4H-SiC polytype in this work.

Various processes can be used with SiC to form oxide layers, such as dry oxidation,[8] wet oxidation,[9] chemical vapor deposition,[10] and pyrogenic oxidation.[11] During the oxidation process, SiO_2 is formed that creates a protective layer on the SiC and impedes further oxidation,[12] which makes the oxidation of SiC considerably more complicated than the oxidation of Si.[3,13,14] It is well known that the oxidation of SiC is a face-terminated oxidation.[15–18] Particularly important is the dependence of the oxidation rates on the crystal orientation, which has significant consequences for non-planar device structures, for instance, the trench design of a U-groove metal-oxide-semiconductor field-effect transistor,[19] where the oxide is located on all crystallographic faces.[2] In this case, the oxide growth thicknesses will vary in the dependence of the particular face, requiring advanced high-accuracy multi-dimensional modeling to correctly predict the oxide formation of the overall device.

In the previous studies, several models and relations were proposed to explain the Si and SiC oxidation kinetics: the Deal-Grove model,[7,20] Massoud's empirical relation,[3,21–23] the interfacial Si emission model,[24] and the Si and C emission model.[25] However, the available models for thermal SiC oxidation are unable to accurately predict oxide growth for two- and three-dimensional structures due to missing orientation dependencies. Additionally, the models suffer from a lack of accuracy for arbitrary crystal directions, which stems from insufficient growth rate coefficients.

Recently, several experimental investigations of SiC thermal oxidation of different crystallographic faces were performed,[3,7,14,26–28] but some of the published time-dependent oxide thicknesses are inconsistent. Certain measurements from different publications vary up to a factor of three for the same material and oxidation environment. Available experimental and theoretical data are currently not providing a full picture of the oxidation parameters to enable further progress in modeling and simulation of SiC-based devices. Nevertheless, a full set of growth rate coefficients is necessary in order to enable the full simulation capability of two- and especially three-dimensional SiC oxidation processes, even if particular growth

a)Electronic mail: simonka@iue.tuwien.ac.at

rates are technologically not feasible. In this case, the gap between technology and simulations cannot be ignored, but to drive technology further, reasonable assumptions of oxide growth for a specific setup via simulations are essential.

In this work, we provide a full set of growth rate coefficients to enable the high-accuracy multi-dimensional simulation of dry 4H-SiC thermal oxidation. These growth rate coefficients stem from a specific set of conditions derived from the experimental data: dry thermal oxidation of *n*-type, on-axis 4H-SiC at atmospheric pressure in the temperature region $900 - 1150\,^{\circ}\mathrm{C}$. We carefully distinguish between the most common crystallographic faces to enable orientation-aware simulations. In order to obtain accurate orientation-dependent growth rate coefficients, we investigate experimental findings and fit the most reasonable time-dependent data with Massoud's empirical relation, as it exhibits the best fit among the available oxidation models. Additionally, we predict the oxidation kinetics for the m-face orientation of 4H-SiC and obtain its oxidation growth rate coefficients. The completed set of oxidation rates enables to augment available process simulation tools and supports a recently proposed anisotropic interpolation method,[29,30] which makes three-dimensional simulations of SiC oxidation possible. Our contributions enable, for the first time, multi-dimensional modeling of orientation- and time-dependent dry thermal oxidation of 4H-SiC and thus enable high-accuracy simulations of the oxide growth on arbitrary SiC structures.

In Section II, we discuss the thermal oxidation process and physical models of Si and SiC oxidation and introduce our fitting method and the temperature-dependent Arrhenius equation. In Section III, we present and discuss time-dependent oxide thicknesses and Arrhenius plots of oxidation growth rates, including activation energies and pre-exponential factors for the four crystal orientations.

II. METHODS

One of the classical oxidation models is the Deal-Grove model[20] that has been originally proposed to describe the Si oxidation process. According to this model, oxidation occurs by diffusion of the oxidant to the SiO_2/Si interface, where it reacts with Si. In the case of dry oxidation, the growth rate in the thin oxide regime ($X < 0.05\,\mu\mathrm{m}$) cannot be reproduced by the Deal-Grove model.[5,6,31] Hence, Massoud *et al.*[21,22] have proposed an empirical modification of the Deal-Grove model to describe the growth rate enhancement in a thin oxide regime. This model introduces an additional exponential term[21,22]

$$\frac{dX}{dt} = \frac{B}{A + 2X} + C\exp\left(-\frac{X}{L}\right), \tag{1}$$

where B/A is the linear rate coefficient, B the parabolic rate coefficient, C an initial enhancement parameter, and L a characteristic length. However, this empirical equation is based on the observations rather than a theory; therefore, it can only reproduce the observed growth rates numerically but cannot provide a theoretical explanation, i.e., physical insight.[13]

The Deal-Grove model and Massoud's empirical relation can be applied to reproduce the SiC oxidation kinetics, as well as to predict the physical mechanisms.[3,7,21,22] The Deal-Grove model, however, can only accurately describe the time-dependent oxidation process for a limited thickness regime.[5] On the contrary, Massoud's empirical relation does not suffer from such a limitation[6] and is thus used in our work to fit the time-dependent experimental data. The processes of SiC oxidation can be presented by time-dependent thicknesses ($X(t)$) or growth rates ($dX/dt(t)$), and/or thickness-dependent growth rates ($dX/dt(X)$).[21,22] For the model fitting, we use a combination of both time-dependent data, i.e., growth rates and thicknesses. The fit to the chosen $X(t)$ data is the primary result, while the fit to the $dX/dt(t)$ data serves as a backup check of the fitting parameters. This approach enables our model fitting to have less than 5% error in the entire time scale of a single fit. In general, for process simulators, e.g., SILVACO's Victory Process,[32] the time-dependent oxide thickness data are of primary importance for accurately predicting structure prototypes. We follow this industry-proven procedure and use the same visualization approach, as is also favored in Song *et al.*[7]

In this study, we use the very well known fourth-order Runge-Kutta method[33,34] to find a numerical approximation for the solution of the ordinary differential equation, as introduced by Massoud's empirical relation. The numerical integration of Massoud's empirical relation includes the following parameters: B/A, B, C, and L, whose values must be carefully set for successfully fitting experimental data. Thus, we have used a fitting algorithm with an auto-step size adjustment to ensure the best fit.[35] The experimental data, i.e., the time-dependent oxide thicknesses during dry SiC oxidation, were obtained from the available publications.[3,7,14,26–28] In order to choose the most reasonable data for fitting, an in-depth analysis of available measurements was performed. In particular, the reference data sets for the same oxidation environments and crystal orientations have been chosen, which yielded conclusive results.

The ratio of the SiC oxidation process highly depends on the temperature. All of the growth rate coefficients B/A, B, C, and L are temperature-dependent. The relation between the absolute temperature T and the rate constant k is given by an Arrhenius equation[36]

$$k = Z\exp\left(-\frac{E_a}{k_B T}\right), \tag{2}$$

where Z is the pre-exponential factor, E_a is the activation energy, and k_B is the Boltzmann constant.

Furthermore, the SiC oxidation process highly depends on the surface orientation.[15–17] We thus carefully distinguish between different crystal orientations: (0001) Si-, $(11\bar{2}0)$ a-, $(1\bar{1}00)$ m-, and $(000\bar{1})$ C-face. According to the recent findings by Goto *et al.*,[3] not all the parameters of Massoud's empirical relation are orientation-dependent. The growth rate B describes the diffusivity in SiO_2; therefore, the nature of the oxide determines the value of B that is identical for all surface orientations.[3] Since converting a SiC molecule into SiO_2 and CO (as in the case for SiC oxidation) consumes 1.5

times the amount of oxygen than converting Si into SiO_2 only (as in the case for Si oxidation), the value of B is assumed to be $1/1.5$ of that of Si[3]

$$B = \frac{2D_O^{SD}}{1.5}, \tag{3}$$

where D_O^{SD} is the oxygen self-diffusivity in SiO_2 for the Si oxidation. Diffusivity is in general temperature-dependent and can be well predicted by an Arrhenius equation[37]

$$D_O^{SD} = D_0 \exp\left(-\frac{E_a^{SD}}{k_B T}\right), \tag{4}$$

where D_0 is the diffusion coefficient and E_a^{SD} is the activation energy. In the case of Si oxidation, $D_0 = 192\,\mu m^2\ min^{-1}$ and $E_a^{SD} = 1.64\,eV$, as reported by Kageshima *et al.*[37] Accordingly, the value of B is assumed to be

$$B = 256 \exp\left(-\frac{1.64\,eV}{k_B T}\right) \mu m^2 min^{-1}. \tag{5}$$

III. RESULTS AND DISCUSSION

In the first subsection, we present the temperature- and orientation-dependent kinetics of 4H-SiC dry thermal oxidation. We compare the published time-dependent oxide thicknesses for the (0001) Si-, the $(11\bar{2}0)$ a-, and the $(000\bar{1})$ C-face SiC substrates and show the obtained fitting results. Additionally, we show predicted oxidation kinetics for the 4H-SiC $(1\bar{1}00)$ m-face. In the second subsection, we present Arrhenius plots for the oxidation growth rate coefficients B/A, B, C, and L. We fit the obtained growth rate coefficients and propose activation energies and pre-exponential factors for all the four crystallographic faces. According to the temperature and orientation dependence of the growth rate coefficients, we discuss the oxidation mechanism.

A. Oxide thicknesses

Figs. 1–4 show our modeling results and experimental data of dry thermal oxidation kinetics of the 4H-SiC (0001) Si-, $(11\bar{2}0)$ a-, $(1\bar{1}00)$ m-, and $(000\bar{1})$ C-face, respectively. There is a large variation in the oxide growth between the different crystallographic faces and various oxidation temperatures, which clearly supports our approach. For any particular oxidation temperature, the oxide thickness is largest for the C-face followed by the m-, the a-, and the Si-face.

The solid lines are fits using Massoud's empirical relation, and the data points are measured values obtained from the studies by Gupta *et al.*,[14] Goto *et al.*,[3] Song *et al.*,[7] Hosoi *et al.*,[26] Kakubari *et al.*,[27] and Shenoy *et al.*[28] The growth of oxide on SiC depends on various factors, e.g., cut-off angle, doping density, and crystal quality, which are the reasons for diverse experimental reports. We observe the highest inconsistencies in the measurements of Si-oriented SiC oxidation, as is clearly seen in Fig. 1. Therefore, we have fitted only the most reasonable data, i.e., the data sets that yield conclusive results for the same oxidation environments and crystal orientations. Our fitted curves are deviating less than 5% from

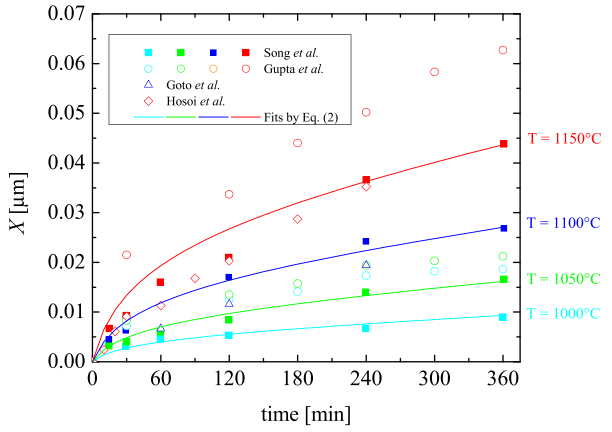

FIG. 1. Oxide thicknesses as a function of time for various temperatures of dry thermal oxidation of the 4H-SiC (0001) Si-face. The solid lines are fits by Eq. (1), the symbols are measurements, and the colours indicate temperatures. A native oxide thickness $X(0) = 2$ Å is used, which is a typical initial condition.[39]

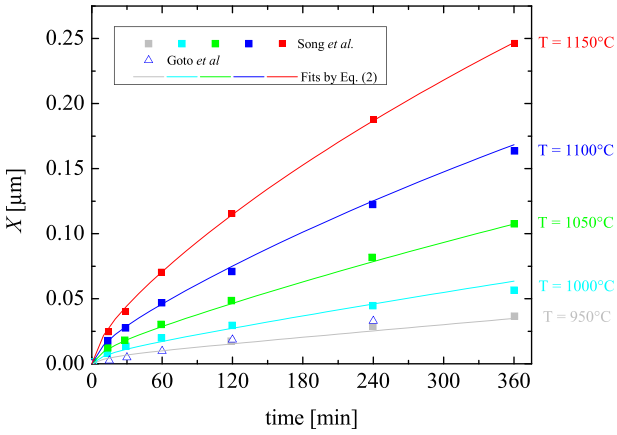

FIG. 2. Oxide thicknesses as a function of time for various temperatures of dry thermal oxidation of the 4H-SiC $(11\bar{2}0)$ a-face. The solid lines are fits by Eq. (1), the symbols are measurements, and the colours indicate various temperatures. A native oxide thickness $X(0) = 2$ Å is used, which is a typical initial condition.[39]

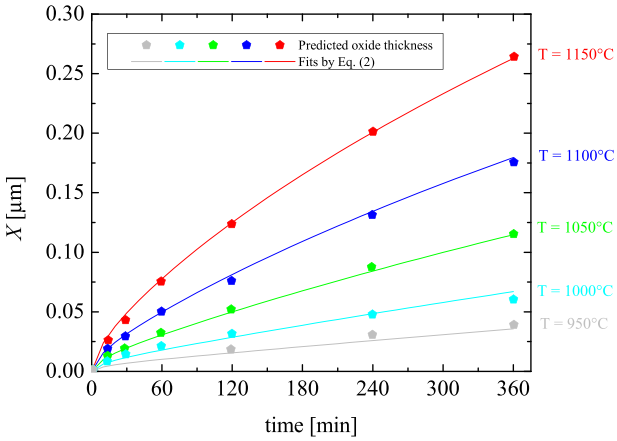

FIG. 3. Oxide thicknesses as a function of time for various temperatures of dry thermal oxidation of the 4H-SiC $(1\bar{1}00)$ m-face. The solid lines are fits by Eq. (1), the symbols are predicted oxide thicknesses, and the colours indicate various temperatures. A native oxide thickness $X(0) = 2$ Å is used, which is a typical initial condition.[39]

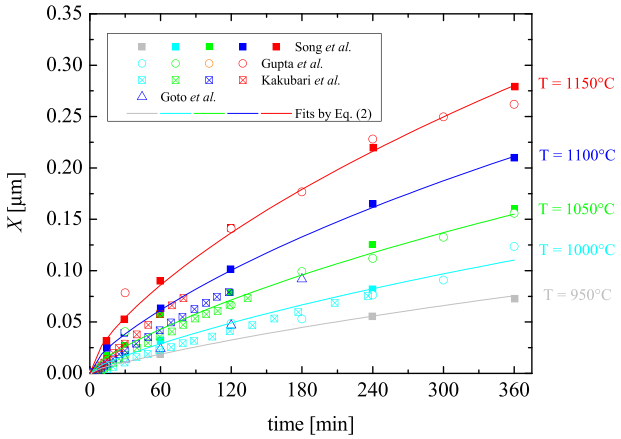

FIG. 4. Oxide thicknesses as a function of time for various temperatures of dry thermal oxidation of the 4H-SiC $(000\bar{1})$ C-face. The solid lines are fits by Eq. (1), the symbols are measurements, and the colours indicate various temperatures. A native oxide thickness $X(0) = 2$ Å is used, which is a typical initial condition.[39]

the chosen measurements in the entire thickness region ($2X \ll A$ and $2X \gg A$), considering different surface orientations and a typical temperature range from 950 to 1150 °C.

As there are no measurement sets available for the $(1\bar{1}00)$ m-face orientation, the oxidation kinetics was predicted (Fig. 3) according to the oxide thicknesses published by Christiansen and Helbig.[38] The prediction is based on the oxide thickness ratio between the m- and a-face $X_{(1\bar{1}00)}(t = 720\,\text{min})/X_{(11\bar{2}0)}(t = 720\,\text{min}) = 1.073$. Accordingly, the m-face kinetics is calculated from the oxidation kinetics of the a-face. A similar approximation was used in our recent study.[29,30]

B. Arrhenius plots

With the fitting procedure discussed in Section II, we have determined the growth rate coefficients of dry 4H-SiC oxidation, i.e., B/A, C, and L. Figs. 5–8 show the temperature

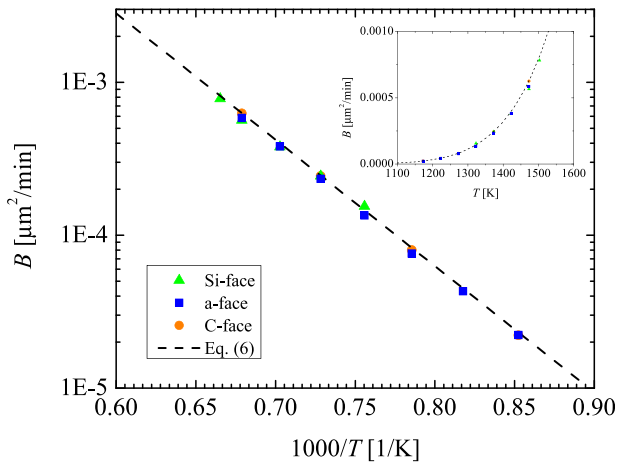

FIG. 5. Arrhenius plots for parabolic growth rate coefficient B for the (0001) Si- (green triangles), the $(11\bar{2}0)$ a- (blue squares), the $(1\bar{1}00)$ m- (red diamonds), and the $(000\bar{1})$ C-face (orange circles) of 4H-SiC dry thermal oxidation. The experimental data for the Si-, the a-, and the C-face (symbols) were obtained from Goto *et al.*,[3] and the fitting dashed lines were calculated with Eq. (5).

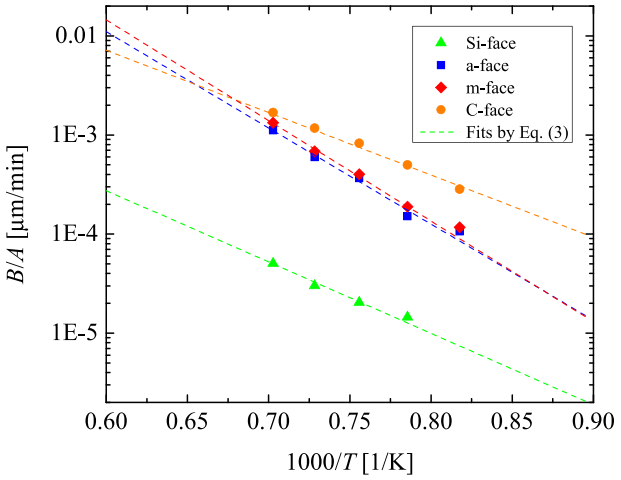

FIG. 6. Arrhenius plots for the linear growth rate coefficient B/A for the (0001) Si- (green triangles), the $(11\bar{2}0)$ a- (blue squares), the $(1\bar{1}00)$ m- (red diamonds), and the $(000\bar{1})$ C-face (orange circles) of 4H-SiC dry thermal oxidation. The rate coefficients at various temperatures (symbols) were obtained by fitting Massoud's empirical relation to the data shown in Figs. 1–4. The dashed lines represent fits by the Arrhenius equation.

dependence of the parabolic growth rate coefficient B, the linear growth rate coefficient B/A, the initial enhancement parameter C, and the characteristic length L, respectively. B/A, C, and L were obtained by fitting the experimental data, as shown in Figs. 1–4. The value of B was obtained from the Si oxidation studies (see Eq. (5)). The linear growth rate coefficient has the largest influence on the final oxide thicknesses, but nevertheless the exponential part of Massoud's empirical relation significantly improves our fitting method and solutions.

In Fig. 6, we observe that the slopes of the Arrhenius plots of the Si- and the C-face are almost identical, i.e., the values of the activation energies E_a are comparable for both orientations. Additionally, the slopes of the Arrhenius plot of the a- and the m-face are almost identical as well. The activation energy of the linear growth rate coefficient defines the

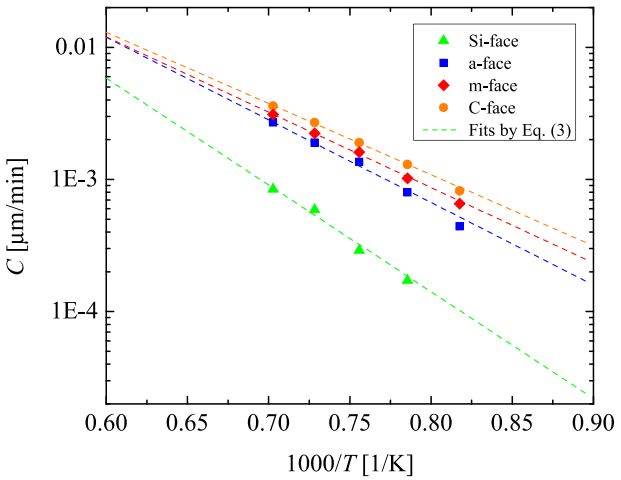

FIG. 7. Arrhenius plots for the initial enhancement parameter C for the (0001) Si- (green triangles), the $(11\bar{2}0)$ a- (blue squares), the $(1\bar{1}00)$ m- (red diamonds), and the $(000\bar{1})$ C-face (orange circles) of 4H-SiC dry thermal oxidation. The rate coefficients at various temperatures (symbols) were obtained by fitting Massoud's empirical relation to the data shown in Figs. 1–4. The dashed lines represent fits by the Arrhenius equation.

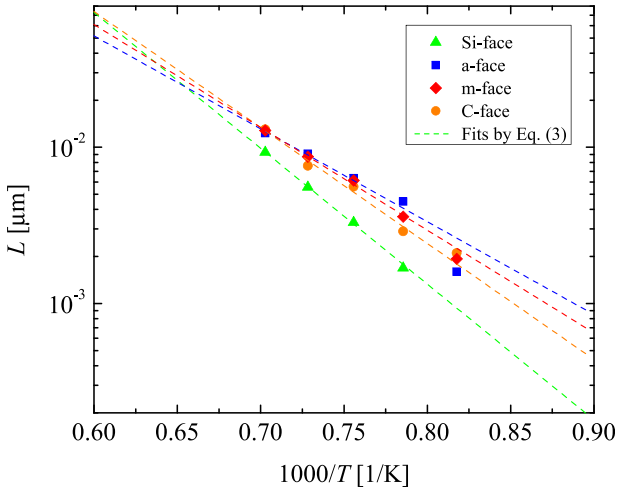

FIG. 8. Arrhenius plots for the characteristic length L for the (0001) Si- (green triangles), the $(11\bar{2}0)$ a- (blue squares), the $(1\bar{1}00)$ m- (red diamonds), and the $(000\bar{1})$ C-face (orange circles) of 4H-SiC dry thermal oxidation. The rate coefficients at various temperatures (symbols) were obtained by fitting Massoud's empirical relation to the data shown in Figs. 1–4. The dashed lines represent fits by the Arrhenius equation.

interfacial reaction rate and is strongly correlated with the crystal structure of the oxidizing surface.[13,14] Therefore, the activation energies are expected to be similar for surfaces with similar structures, which is verified by our results. By careful examination of the 4H-SiC structure, as shown in Fig. 9, we notice that the crystal structure is almost identical for the Si-face (top) and the C-face (bottom), as well as for the a- (one side) and the m-face (another side of the crystal). Comparing this with the thermal oxidation of Si, the interface chemical reaction is almost the same for the Si- and the C-face.[40] Nevertheless, the oxidation growth rates for the Si- and the C-face are different, as the areal density of atoms and the mechanical stress effects at the interface play a crucial role in the oxidation, which can be explained by the magnitude of the pre-exponential factor of the linear growth rate coefficient.[7] This is in agreement with our results, where the differences in the growth rates of the Si- and the C-face are mainly significant in the pre-exponential factor Z, which is an order of magnitude larger for the C-face compared to the Si-face. Fig. 6 also shows that the activation energies of the m- and the a-face are higher than the activation energies of the C- and the Si-face. Additionally, the results in the Fig. 6 suggest that the difference of the linear growth rate coefficient between the a- and the m-face is negligible for low temperature regime, which is in agreement with Tokura *et al.*[19]

Fig. 7 shows that the growth rate enhancement parameter for thin oxides for all four crystallographic faces is temperature-dependent. The results suggest that the initial oxidation growth rate is highest for the C-, followed by the m-, a-, and the Si-face orientations. By comparing the results of Figs. 6 and 7, it is clear that the ratios of the growth rates between the four crystallographic faces are different, which suggests that the temperature dependence of the initial and the linear growth rates is diverse. The values of B/A are in the same order of magnitude than the values of C; hence, the contribution of the initial oxide growth enhancement cannot be neglected. This fact is in alignment with the already established knowledge that the Deal-Grove model cannot accurately predict the oxidation kinetics for SiC.[5,6]

The results in Fig. 8 suggest that the characteristic length L is also temperature- and orientation-dependent. L is determined by the oxidation and the diffusion coefficient of SiO_2 interstitials and the emission ratios of Si and C interstitials. An increase in the diffusion leads to an increase in L, while an increase in the oxidation coefficient or the emission ratio of interstitials leads to a reduction in L.[3] The results in Fig. 8 are consistent with the reports from Goto *et al.*[3] and Uematsu *et al.*,[41] who suggest that a temperature increase is more significant for the diffusion coefficient than the

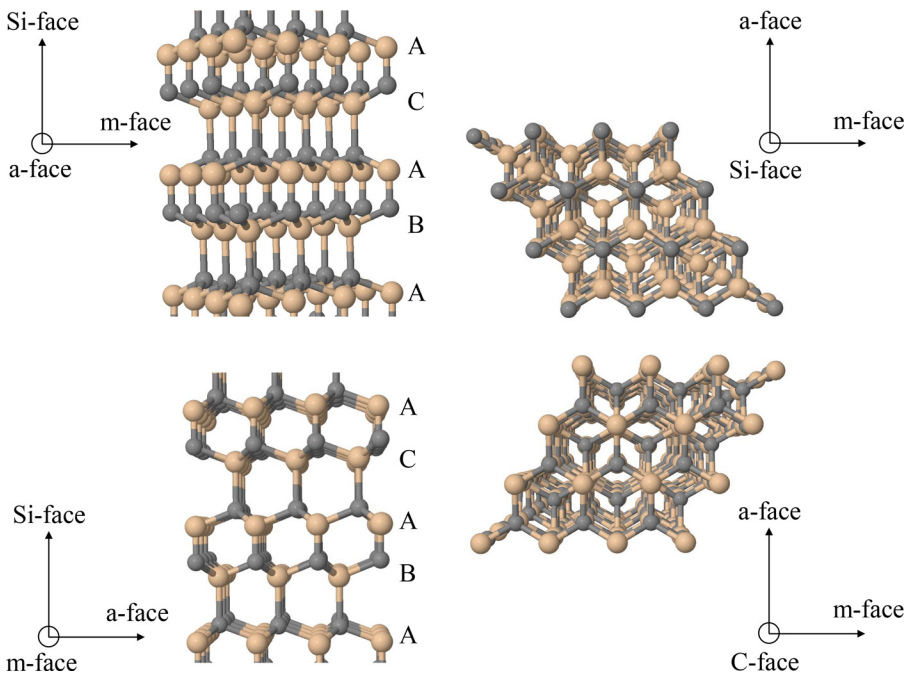

FIG. 9. Atomistic three-dimensional schematic illustrations of various perspectives of a 4H-SiC polytype with the stacking sequence ABAC. Orange spheres represent Si atoms, gray spheres C atoms, and arrows showing directions towards corresponding crystallographic faces.

oxidation coefficient or emission ratios. We observe higher values of L for the C-face orientation than for the Si-face for the temperature regime below 1265 °C, which is consistent with the predictions that the emission ratio for the Si-face is significantly larger than that for the C-face.[42,43] Interestingly, we observe higher values of L for the m- and the a-face than the ones for the C-face for $T < 1265$ °C, i.e., the initial growth enhancement is larger for the m- and the a-face for this temperature regime. We believe that the reason for this phenomenon is a higher diffusion coefficient, lower emission ratio, and lower oxidation coefficient of the m- and the a-face compared to the C-face. The results in Fig. 8 also suggest that the mentioned relations are reversed for the temperature regime above 1265 °C. Additionally, the differences in L between the Si- and the C-face at very high oxidation temperatures are lower than 5%. Therefore, in the high temperature region, the value of L for both the faces is approximately the same.

In general, the parameters obtained in this study show some differences from the parameters reported previously by Goto *et al.*[3] and Song *et al.*[7] This is expected as we use a more advanced oxidation model, i.e., we use Massoud's empirical relation instead of the Deal-Grove model and we apply our fitting method to carefully selected experimental data (see Section II), i.e., different data sets than in the study by Goto *et al.*[3] The largest differences in the obtained parameters are seen especially in the oxidation of the 4H-SiC Si-face. These inequalities are derived from the initial data sets of oxidation kinetics of Si-oriented SiC. On the other hand, the two other orientations, C- and a-face, show conclusive results that are in line with the findings of Goto *et al.*[3] For m-oriented SiC, there are no comparisons possible yet, as these are the first proposed parameters for dry thermal oxidation of 4H-SiC m-face. Overall, the growth rates obtained in this study show excellent results in process simulations with SILVACO's Victory Process[32] with respect to the experimental findings[19,38] (see follow-up results[44]).

Table I provides an overview of the obtained activation energies and the pre-exponential factors of Arrhenius plots for all the four inspected crystallographic faces. As discussed before, the pre-exponential factor has a significant role in the temperature dependence of the SiC oxidation kinetics; therefore, it is always necessary to present Arrhenius plots, considering E_a together with Z.

Using our computed and validated parameters (see Table I), we are able to accurately simulate multi-dimensional 4H-SiC oxidation kinetics. Fig. 10 shows predicted oxidation growth rates as a function of oxide thicknesses for the Si-, the a-, the m-, and the C-face at various relevant temperatures, which are $T = 950$, 1000, 1050, 1100, and 1150 °C. The simulations suggest that the initial enhancement of the oxide growth is strongest for the Si-face. Furthermore, at low temperatures, the differences in the growth rates between the m- and the a-face orientations are less than 5%. Additionally, the growth rate of the C-face is significantly larger compared to the other orientations at low temperatures: e.g., $T = 950$ °C, the average growth rates for the Si-, the a-, the m- and the C-face are 0.12×10^{-4}, 0.90×10^{-4}, 0.93×10^{-4}, and 1.82×10^{-4} μm/min, respectively. On the other hand, this difference is less distinct at higher temperatures: e.g., $T = 1150$ °C, the average growth rates for the Si-, the a-, the m- and the C-face are 0.93×10^{-4}, 5.70×10^{-4}, 6.02×10^{-4}, and 6.39×10^{-4} μm/min, respectively.

The saturation of the oxidation process depends on the temperature and pressure, as well as on the chemical nature of the substances. The derivatives of the curves shown in Fig. 10 indicate that the saturation of the oxide growth is highest, i.e., the oxidation process is hindered the most for the Si-oriented SiC. This is consistent with the previous reports from Goto *et al.*,[3] Yamamoto *et al.*,[5] and Hijikata *et al.*[25] The results also indicate that the saturation of SiC oxidation is orientation-dependent.

TABLE I. Activation energies and pre-exponential factors of the Arrhenius plots for the (0001) Si-, the $(11\bar{2}0)$ a-, the $(1\bar{1}00)$ m-, and the $(000\bar{1})$ C-face of 4H-SiC dry thermal oxidation. The linear rate coefficient B/A, the initial enhancement parameter C, and the characteristic length L were obtained by fitting Eq. (2) to the data presented in Figs. 6–8.

	B/A		C		L	
	E_a (eV)	Z (μm/min)	E_a (eV)	Z (μm/min)	E_a (eV)	Z (μm)
Si-face	1.429	5.751	1.604	412.9	1.724	1.190×10^4
a-face	1.927	7.404×10^3	1.241	67.51	1.180	189.5
m-face	2.015	1.791×10^4	1.132	31.84	1.305	539.8
C-face	1.249	42.70	1.069	22.22	1.473	2.096×10^3

IV. CONCLUSIONS

The temperature- and orientation-dependent dry thermal oxidation of 4H-SiC (0001) Si-, $(11\bar{2}0)$ a-, $(1\bar{1}00)$ m-, and $(000\bar{1})$ C-face has been investigated. We have evaluated the published experimental findings and fitted them with Massoud's empirical relation to obtain the oxidation growth rate coefficients B/A, C, and L for various temperatures, while B was obtained theoretically. In order to introduce temperature dependence, we have fitted the growth rate coefficients with the Arrhenius equation to obtain activation

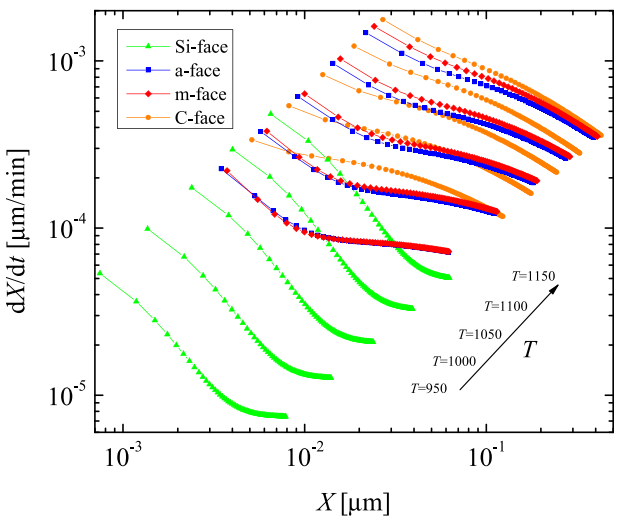

FIG. 10. Oxide growth rates as a function of oxide thicknesses at various temperatures for the (0001) Si- (green triangles), the $(11\bar{2}0)$ a- (blue squares), the $(1\bar{1}00)$ m- (red diamonds), and the $(000\bar{1})$ C-face (orange circles) of 4H-SiC dry thermal oxidation.

energies and pre-exponential factors for each crystal orientation. Interface reaction rates are similar for the Si- and the C-face as well as for the a- and the m-face, but for these orientations the areal density of atoms and the mechanical stress effects are different. The initial enhancement parameter C cannot be neglected, as it is in the same order of magnitude as the linear growth rate coefficient B/A. The characteristic length L shows a higher diffusion coefficient, lower emission ratio, and lower oxidation coefficient for the m- and the a-face compared to the C-face. All of the growth rates play an important role in the oxidation anisotropy of SiC. From the predicted oxidation growth rates as a function of oxide thicknesses, we observe that the saturation of the oxide growth is highest for the Si-face and that the initial oxide enhancement is strongest for the m- and the a-face. Overall, the parameters from this work, together with the recently proposed interpolation method,[29,30] enable high-accuracy multi-dimensional simulations of dry thermal oxidation of 4H-SiC.

ACKNOWLEDGMENTS

The financial support by the Austrian Federal Ministry of Science, Research and Economy and the National Foundation for Research, Technology and Development is gratefully acknowledged.

[1]G. L. Harris, *Properties of Silicon Carbide* (INSPEC, United Kingdom, 1995).
[2]C. Harris and V. Afanas'ev, "SiO_2 as an insulator for SiC devices," Microelectron. Eng. **36**, 167–174 (1997).
[3]D. Goto, Y. Hijikata, S. Yagi, and H. Yaguchi, "Differences in SiC thermal oxidation process between crystalline surface orientations observed by *in-situ* spectroscopic ellipsometry," J. Appl. Phys. **117**, 095306 (2015).
[4]Y. Hijikata, H. Yaguchi, S. Yoshida, Y. Takata, K. Kobayashi, H. Nohira, and T. Hattori, "Characterization of oxide films on 4H-SiC epitaxial (0001) faces by high-energy-resolution photoemission spectroscopy: Comparison between wet and dry oxidation," J. Appl. Phys. **100**, 053710 (2006).
[5]T. Yamamoto, Y. Hijikata, H. Yaguchi, and S. Yoshida, "Oxide growth rate enhancement of silicon carbide (0001) Si-faces in thin oxide regime," Jpn. J. Appl. Phys., Part 1 **47**, 7803 (2008).
[6]T. Yamamoto, Y. Hijikata, H. Yaguchi, and S. Yoshida, "Growth rate enhancement of (0001)-face silicon–carbide oxidation in thin oxide regime," Jpn. J. Appl. Phys., Part 2 **46**, L770 (2007).
[7]Y. Song, S. Dhar, L. C. Feldman, G. Chung, and J. R. Williams, "Modified deal grove model for the thermal oxidation of silicon carbide," J. Appl. Phys. **95**, 4953–4957 (2004).
[8]I. Vickridge, J. Ganem, Y. Hoshino, and I. Trimaille, "Growth of SiO_2 on SiC by dry thermal oxidation: Mechanisms," J. Phys. D: Appl. Phys. **40**, 6254 (2007).
[9]H. Yano, F. Katafuchi, T. Kimoto, and H. Matsunam, "Effects of wet oxidation/anneal on interface properties of thermally oxidized SiO_2/SiC MOS system and MOSFET's," IEEE Trans. Electron. Devices **46**, 504–510 (1999).
[10]K. Kamimura, D. Kobayashi, S. Okada, T. Mizuguchi, E. Ryu, R. Hayashibe, F. Nagaune, and Y. Onuma, "Preparation and characterization of SiO_2/6H–SiC metal–insulator–semiconductor structure using TEOS as source material," Appl. Surf. Sci. **184**, 346–349 (2001).
[11]P. Lai, J. Xu, H. Wu, and C. Chan, "Interfacial properties and reliability of SiO_2 grown on 6H-SiC in dry O_2 Plus trichloroethylene," Microelectron. Reliab. **44**, 577–580 (2004).
[12]D. A. Newsome, D. Sengupta, H. Foroutan, M. F. Russo, and A. C. van Duin, "Oxidation of silicon carbide by O_2 and H_2O: A ReaxFF reactive molecular dynamics study, Part I," J. Phys. Chem. C **116**, 16111–16121 (2012).
[13]Y. Hijikata, *Physics and Technology of Silicon Carbide Devices* (InTech, Croatia, 2013).
[14]S. K. Gupta and J. Akhtar, *Thermal Oxidation of Silicon Carbide (SiC)-Experimentally Observed Facts* (INTECH, China, 2011).
[15]M. Schürmann, S. Dreiner, U. Berges, and C. Westphal, "Structure of the interface between ultrathin SiO_2 films and 4H-SiC (0001)," Phys. Rev. B **74**, 035309 (2006).
[16]P. Fiorenza and V. Raineri, "Reliability of thermally oxidized SiO_2/4H-SiC by conductive atomic force microscopy," Appl. Phys. Lett. **88**, 212112 (2006).
[17]T. Yamamoto, Y. Hijikata, H. Yaguchi, and S. Yoshida, "Oxygen-partial-pressure dependence of SiC oxidation rate studied by *in situ* spectroscopic ellipsometry," in *Proceedings of Materials Science Forum* (2009), pp. 667–670.
[18]J. J. Ahn, Y. D. Jo, S. C. Kim, J. H. Lee, and S. M. Koo, "Crystallographic plane-orientation dependent atomic force microscopy-based local oxidation of silicon carbide," Nanoscale Res. Lett. **6**, 1–5 (2011).
[19]N. Tokura, K. Hara, T. Miyajima, H. Fuma, and K. Hara, "Current-voltage and capacitance-voltage characteristics of metal/oxide/6H-silicon carbide structure," Jpn. J. Appl. Phys., Part 1 **34**, 5567 (1995).
[20]B. E. Deal and A. Grove, "General relationship for the thermal oxidation of silicon," J. Appl. Phys. **36**, 3770–3778 (1965).
[21]H. Z. Massoud, J. D. Plummer, and E. A. Irene, "Thermal oxidation of silicon in dry oxygen growth-rate enhancement in the thin regime I. Experimental results," J. Electrochem. Soc. **132**, 2685–2693 (1985).
[22]H. Z. Massoud, J. D. Plummer, and E. A. Irene, "Thermal oxidation of silicon in dry oxygen: Growth-rate enhancement in the thin regime II. Physical mechanisms," J. Electrochem. Soc. **132**, 2693–2700 (1985).
[23]H. Z. Massoud, J. D. Plummer, and E. A. Irene, "Thermal oxidation of silicon in dry oxygen accurate determination of the kinetic rate constants," J. Electrochem. Soc. **132**, 1745–1753 (1985).
[24]H. Kageshima, K. Shiraishi, and M. Uematsu, "Universal theory of Si oxidation rate and importance of interfacial Si emission," Jpn. J. Appl. Phys., Part 2 **38**, L971 (1999).
[25]Y. Hijikata, H. Yaguchi, and S. Yoshida, "A kinetic model of silicon carbide oxidation based on the interfacial silicon and carbon emission phenomenon," Appl. Phys. Express **2**, 021203 (2009).
[26]T. Hosoi, D. Nagai, T. Shimura, and H. Watanabe, "Exact evaluation of interface-reaction-limited growth in dry and wet thermal oxidation of 4H-SiC (0001) Si-face surfaces," Jpn. J. Appl. Phys., Part 1 **54**, 098002 (2015).
[27]K. Kakubari, R. Kuboki, Y. Hijikata, H. Yaguchi, and S. Yoshida, "Real time observation of SiC oxidation using an in situ ellipsometer," in *Proceedings of Materials Science Forum* (2006), pp. 1031–1034.
[28]J. Shenoy, M. Das, J. Cooper, Jr., M. Melloch, and J. Palmour, "Effect of substrate orientation and crystal anisotropy on the thermally oxidized SiO_2/SiC Interface," J. Appl. Phys. **79**, 3042–3045 (1996).
[29]V. Šimonka, G. Nawratil, A. Hössinger, J. Weinbub, and S. Selberherr, "Anisotropic interpolation method of silicon carbide oxidation growth rates for three-dimensional simulation," Solid-State Electron. (unpublished).
[30]V. Šimonka, G. Nawratil, A. Hössinger, J. Weinbub, and S. Selberherr, "Direction dependent three-dimensional silicon carbide oxidation growth rate calculations," in *Proceedings of 2016 Joint International EUROSOI Workshop and International Conference on Ultimate Integration on Silicon* (2016), pp. 226–229.
[31]A. S. Grove, *Physics and Technology of Semiconductor Devices* (Wiley, United Kingdom, 1967).
[32]See http://www.silvaco.com/products/tcad/process_simulation/victory_process/victory_process.html for victory process.
[33]D. Potter, *Computational Physics* (Wiley, United Kingdom, 1973).
[34]J. Thijssen, *Computational Physics* (Cambridge University Press, United Kingdom, 2007).
[35]R. Macey, G. Oster, and T. Zahley, *Berkeley Madonna Users Guide* (University of California, Berkely, CA, 2009).
[36]S. Arrhenius, *Über die Dissociationswärme und den Einfluss der Temperatur auf den Dissociationsgrad der Elektrolyte* (Wilhelm Engelmann, Germany, 1889).
[37]H. Kageshima, M. Uematsu, and K. Shiraishi, "Theory of thermal si oxide growth rate taking into account interfacial si emission effects," Microelectron. Eng. **59**, 301–309 (2001).
[38]K. Christiansen and R. Helbig, "Anisotropic oxidation of 6H-SiC," J. Appl. Phys. **79**, 3276–3281 (1996).
[39]S. Dhar, Y. Song, L. Feldman, T. Isaacs-Smith, C. Tin, J. Williams, G. Chung, T. Nishimura, D. Starodub, T. Gustafsson *et al.*, "Effect of nitric oxide annealing on the interface trap density near the conduction bandedge

of 4H-SiC at the oxide/(1120) 4H-SiC interface," Appl. Phys. Lett. **84**, 1498–1500 (2004).
[40]E. A. Irene, H. Z. Massoud, and E. Tierney, "Silicon oxidation studies: Silicon orientation effects on thermal oxidation," J. Electrochem. Soc. **133**, 1253–1256 (1986).
[41]M. Uematsu, H. Kageshima, and K. Shiraishi, "Simulation of wet oxidation of silicon based on the interfacial silicon emission model and comparison with dry oxidation," J. Appl. Phys. **89**, 1948–1953 (2001).
[42]Y. Hijikata, H. Yaguchi, and S. Yoshida, "Model calculations of SiC oxide growth rate at various oxidation temperatures based on the silicon and carbon emission model," in *Proceedings of Materials Science Forum* (2010), pp. 809–812.
[43]Y. Hijikata, H. Yaguchi, and S. Yoshida, "Theoretical studies for si and c emission into SiC layer during oxidation," in *Proceedings of Materials Science Forum* (2011), pp. 429–432.
[44]V. Šimonka, A. Hössinger, J. Weinbub, and S. Selberherr, "Three-dimensional growth rate modeling and simulation of silicon carbide thermal oxidation," in *Proceedings of 2016 International Conference on Simulation of Semiconductor Processes and Devices (SISPAD)* (2016), pp. 233–237.